

# How Quorum Sensing Shapes Clustering in Active Matter

L. de Souza<sup>1,2,\*</sup> E. F. Teixeira<sup>3,†</sup> G. M. Viswanathan<sup>1,4,‡</sup> P. Sollich<sup>2,5,§</sup> and P. de Castro<sup>6,¶</sup>

<sup>1</sup>*Departamento de Física Teórica e Experimental,  
Universidade Federal do Rio Grande do Norte. Natal 59078-970, Brazil*

<sup>2</sup>*Institut für Theoretische Physik, University of Göttingen,  
Friedrich-Hund-Platz 1, 37077 Göttingen, Germany*

<sup>3</sup>*Instituto de Física, Universidade Federal do Rio Grande do Sul. Porto Alegre 91501-970, Brazil*

<sup>4</sup>*National Institute of Science and Technology of Complex Systems. Rio de Janeiro 22290-180, Brazil*

<sup>5</sup>*Department of Mathematics, King's College London. London WC2R 2LS, UK*

<sup>6</sup>*ICTP South American Institute for Fundamental Research,  
Instituto de Física Teórica, Universidade Estadual Paulista– UNESP, São Paulo, Brazil*

(Dated: December 3, 2025)

Self-propelled particles undergoing persistent motion can accumulate either through excluded-volume interactions or through quorum sensing, where self-propulsion decreases at high local density. Using kinetic balance theory and simulations, we show that the interplay of these two mechanisms produces a reentrant, non-monotonic behavior in which clustering passes through a pronounced minimum as quorum-sensing strength or persistence time varies. Beyond a threshold quorum sensing strength, we find long-lived transient states that retain memory of initial conditions, including kinetically arrested active gels. Although quorum sensing can mimic attractive interactions, it also acts strongly in dilute regions, producing an effective cluster bistability that is captured by our theory. Our results explain collective states observed experimentally in synthetic and biological active systems.

*Introduction*—Active matter refers to nonequilibrium systems composed of large ensembles of self-propelled entities [1–3], such as bacteria [4], cell tissues [5, 6], animal flocks [7], and colloids [8]. When the directions of self-propulsion fluctuate slowly, the interplay of repulsive contact forces and persistent motion can generate a clustering phenomenon known as motility-induced phase separation (MIPS) [9–12]. This minimal set of ingredients explains the behavior of many synthetic active systems [8, 13]. However, organisms often interact via chemical signals that regulate self-propulsion through a mechanism called quorum sensing (QS) [14–18], which can help survival [19]. Experiments with bacteria, ants, and mussels show that, at moderate densities, QS can suppress contact-force MIPS [14, 17, 20, 21]. Recent experiments with synthetic QS rods [22] and simulations of QS disks [23] showed that the interplay of QS and steric repulsion leads to arrested dynamics and shapes clustering. For simplicity, most models include either steric forces or QS, but rarely both [24–26], which limits their applicability.

A common effective description of QS incorporates motility regulation via a self-propulsion speed that decreases with the local density of individuals, without explicitly modeling signaling molecules [27]. In coarse-grained approaches, this type of QS motility reduction can lead to an effective attraction [28, 29]. For truly attractive active particles, persistent motion can counterbalance attraction, leading instead to homogeneous states [30]. This competition produces a *reentrant* clustering phase diagram: as activity is varied, clustering disappears and then reappears [31–34]. How such reentrant behavior manifests in QS particles remains unclear.

More generally, although a few works have included both QS and steric interactions [22, 23, 35–37], the clustering behavior of these ubiquitous systems is an open problem.

Here, we demonstrate that combining steric repulsion with quorum-sensing motility reduction leads to a reentrant clustering behavior, where a previously unexplored class of active kinetically-arrested *gels* arises [30]. These are disordered solid-like percolating networks [38, 39] which are induced here by QS. Furthermore, QS not only mimics attractive potentials but also induces pronounced effects in dilute regions, which qualitatively transform the phase diagram. Beyond numerical simulations, we derive a kinetic balance theory for the clustering degree by modifying the approach of Ref. [30]. The proposed theory predicts that, depending on the initial condition, different effective equilibria arise. This prediction is confirmed in simulations and resembles behaviors observed in mussel-bed experiments [14, 40]. Taken together, our results bridge synthetic and biological realizations of active matter, demonstrating how quorum sensing, often neglected in modeling efforts, plays a central role in shaping collective organization.

*Model*—We consider  $N$  active Brownian particles (ABPs) in two dimensions with periodic boundary conditions. Their dynamics is

$$\dot{\mathbf{r}}_i(t) = v[\tilde{\rho}(\mathbf{r}_i)] \hat{\mathbf{e}}_i + \mu \sum_{j \neq i} \mathbf{F}_{ij} + \sqrt{2D_T} \boldsymbol{\xi}_i(t), \quad (1)$$

$$\dot{\theta}_i(t) = \sqrt{2D_R} \eta_i(t), \quad (2)$$

where  $\mathbf{r}_i$  is the position,  $\hat{\mathbf{e}}_i = (\cos \theta_i, \sin \theta_i)$  is the self-propulsion direction (or polarity),  $\mu$  is the mobility,  $\xi_{i,x}$ ,

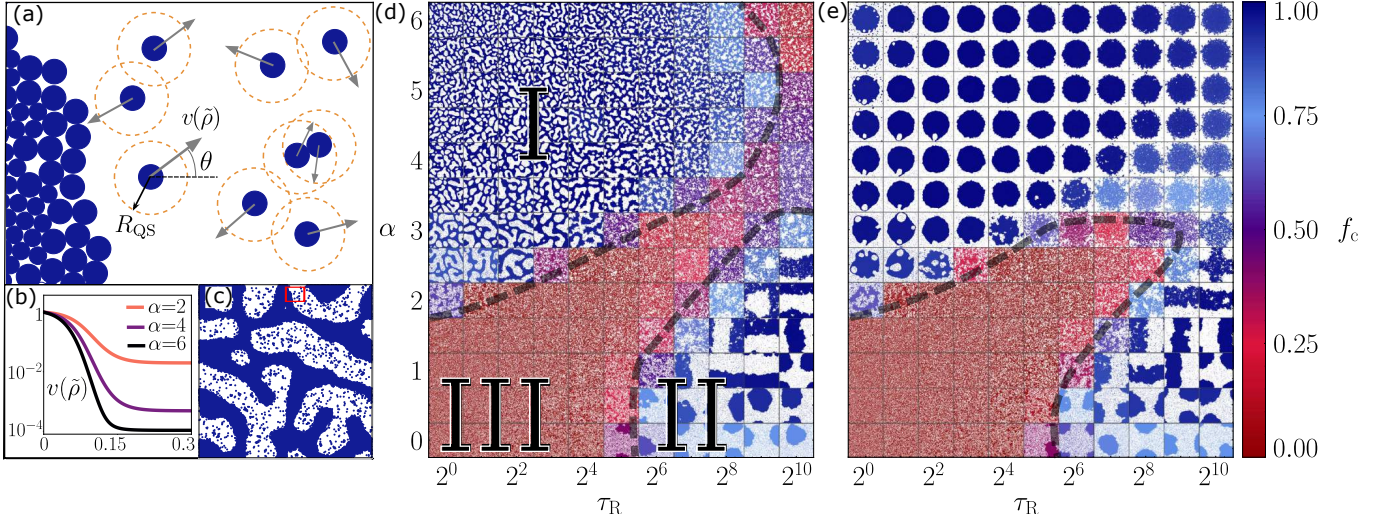


FIG. 1: Quorum sensing gives rise to active gels, reentrant clustering, and long-lived transients. (a) Disk-like particles form an arrested cluster and a dilute phase. Each particle self-propels in a direction defined by  $\theta$  (gray arrows), with a speed  $v$  that decreases with the weighted density  $\tilde{\rho}$  of particles within a radius  $R_{QS}$ . (b)  $v(\tilde{\rho})$  [Eq. (3)] drops from one plateau to another (c) Zoom-out of panel (a) reveals a gel pattern caused by low directional persistence and speeds. Here,  $\tau_R = 4$ ,  $\alpha = 3$ ,  $\phi = 0.4$ ,  $N = 2 \times 10^4$ , and  $t = 2 \times 10^6$ . (d) Phase diagram in the  $\tau_R$ - $\alpha$  plane, based on snapshots at  $t = 2 \times 10^6$  from a homogeneous initial condition. The color bar shows  $f_c$ , averaged between  $t = 1.7 \times 10^6$  and  $2 \times 10^6$ . A reentrant  $f_c$  reveals three regions. Region I shows gels as in panel (c). Region II features motility-induced phase separation due to contact forces. In Region III, slowed particles have just enough persistence to escape without forming clusters. (e) Same as panel (d), but the initial condition is a single cluster with inward-pointing particles at the interface. There is a long-lived transient due to the memory of the initial condition. The diagram in panel (e) converges slowly to that in panel (d); see Supplementary Material [41].

$\xi_{i,y}$ , and  $\eta_i$  are independent unit Gaussian white noises, and  $D_T$  and  $D_R$  are the translational and rotational noise strengths, respectively, treated as independent parameters. We assume strong elastic repulsive contact forces  $\mathbf{F}_{ij} = k (d_{ij} - r_{ij}) \Theta(d_{ij} - r_{ij}) \hat{\mathbf{r}}_{ij}$ , where  $d_{ij} = R_i + R_j$  and  $R_i$  are the particle radii. To avoid artificial crystallization, each particle is randomly assigned one of two radii. The average diameter is  $\sigma = 1$  and the ratio between radii is 1.4 [42]. We work at a moderate packing fraction  $\phi = 0.4$  (that is, number density  $\rho_0 \approx 0.49$ ), with  $N = 2 \times 10^4$  particles.

The quorum-sensing motility regulation is modeled by a density-dependent self-propulsion speed [27]

$$v(\tilde{\rho}) = v_1 + (v_0 - v_1) \exp(-\alpha \mathcal{S}(\tilde{\rho})), \quad (3)$$

where  $\tilde{\rho}$  is a particle density calculated within a QS range,  $R_{QS}$ , around the focal particle; see Fig. 1a and Movie S1 in the Supplementary Material (SM) [41]. Each particle inside the QS range contributes to  $\tilde{\rho}$  with a weight that depends on its distance, as specified by a kernel function given in the SM [41]. Moreover,  $\alpha$  is dubbed QS strength,  $v_0$  is the self-propulsion speed without QS and  $v_1$  for infinite  $\alpha$ , with  $v_0 > v_1$ . Also,  $\mathcal{S}(\tilde{\rho}) = \tanh\left(\frac{\tilde{\rho} - \bar{\rho}}{\delta \rho}\right) + \tanh\left(\frac{\bar{\rho}}{\delta \rho}\right)$  is a sigmoid function [18, 27, 43]. This choice for  $v(\tilde{\rho})$  resembles activation and saturation

effects of chemical receptors in microorganisms. Around  $\tilde{\rho} = \bar{\rho}$ ,  $v(\tilde{\rho})$  undergoes a crossover between two limiting values; see Fig. 1b. How strongly  $v(\tilde{\rho})$  decays depends on the QS strength  $\alpha$  and the decay width  $\delta \rho$ . The polarity persistence time is  $\tau_R \equiv D_R^{-1}$ . We vary  $\alpha$  and  $\tau_R$  and fix the other parameters. For additional simulation details and fixed parameter values, see SM [41]. In particular, we employ  $D_T \ll v_0^2 \tau_R$  and  $v_1 \ll v_0$  as observed for real microorganisms [18, 19, 44]. Nevertheless,  $D_T$  and  $v_1$  still serve to eventually break kinetic arrest in our long simulations.

*Reentrant behavior and effective equilibria*—First, we employ a homogeneous initial condition. To estimate clustering, we calculate the fraction of particles in clusters,  $f_c$ . We consider two particles to be “connected” when  $r_{ij} < 1.1d_{ij}$ . A cluster is defined as any connected group containing more than 5% of all particles. Figure 1d shows a phase diagram in the  $\tau_R$ - $\alpha$  plane based on snapshots at a late time. Each snapshot is colored according to  $f_c$ . The phase diagram displays three regions: two associated with strong clustering ( $f_c \approx 1$ ) and, in between them, a region characterized by nearly homogeneous states ( $f_c \approx 0$ ). Owing to this non-monotonic  $f_c$ , the phase diagram is said to be reentrant. In fact, two distinct reentrant behaviors appear: one upon varying  $\tau_R$  and another upon varying  $\alpha$ .

With the aim of understanding the origin of this phase diagram, let us consider what happens to a particle at the edge of a cluster. For low  $\tau_R$  and high  $\alpha$ , even if the particle is oriented away from the cluster, its self-propulsion speed is too small to allow for the particle to escape before it reorients back toward the cluster. As a result, particles undergo a slow coarsening process, phase-separating into a gas and a kinetically arrested gel [38], where particles are almost static; see Fig. 1c and Movie S2 in the SM [41]. This active gel state arises in Region I of Fig. 1d. Whereas gelation is typically driven by attractive interactions [30], here it emerges through a QS-induced route. By contrast, a distinct route to active gelation without attraction has been reported for particles with non-convex shapes [45].

In the opposite limit of high  $\tau_R$  and low  $\alpha$ , we observe conventional MIPS driven by persistent motion and steric contact repulsion [46], as shown in Region II. The critical value of  $\tau_R$  for the transition to Region II increases with  $\alpha$ , since stronger QS reduces the propulsion speed and thus requires higher persistence to sustain contact-force MIPS. In Region III, particles escape QS but fail to undergo MIPS, resulting in a nearly homogeneous state. The III-II transition was first reported for QS disks in Ref. [37], but for their parameters Region I was not observed. For non-QS attractive particles, Refs. [30, 32] identified a reentrant behavior, with a region in their phase diagrams that resembles Region I. As we demonstrate below, however, QS interactions in dilute regions of the system give rise to effects beyond those observed with attractive interactions.

Because kinetics are slow in Region I, we test the effect of initial conditions by starting from a compact circular cluster with interface particles pointing inward. Fig. 1e shows that, for low  $\alpha$ , the phase diagram is unchanged, while at high  $\alpha$ , a strong QS slowing-down traps particles, producing long-lived clusters. At high  $\tau_R$ , some particles eventually escape, leading to rearrangements that make clusters less compact, though no homogeneous state appears now. At low  $\tau_R$ , the cluster persists but develops holes. This is because particles escape and then reattach at random locations, nucleating finger-like protrusions that slowly merge with each other, thus leaving holes that are the precursors of a gel-like structure.

On extremely long timescales [47], memory of the initial condition ultimately vanishes, with  $f_c$  converging to similar final values for both initial preparations (see SM [41] for longer simulations, including Movie S3). At such long times, for high  $\tau_R$  and  $\alpha$ , particles can eventually escape, collide in the gas phase, and assemble into long-lived microclusters. The original cluster then fully dissipates and reorganizes into a nearly homogeneous state. Because these relaxation times are practically inaccessible, we describe the system in terms of two *effective* equilibria, a perspective that emerges intrinsically in our theory below, that is, without being imposed. Notably,

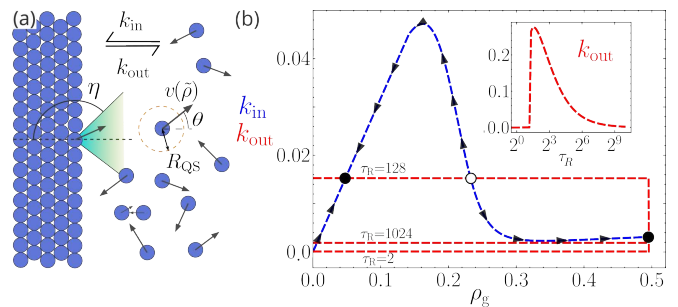


FIG. 2: QS effects on the cluster surface and in the gas explain reentrant clustering and initial-condition dependence. (a) Schematics showing effective escape cone: due to an effective attraction, interface particles pointing outside the cone lack sufficient horizontal self-propulsion to escape. (b)  $k_{\text{in}}$  (blue) and  $k_{\text{out}}$  (red) vs.  $\rho_g$  [Eqs. (4) and (7)] for  $\alpha = 2$  and  $\tau_R = 2, 128$ , and  $1024$ . Inset:  $k_{\text{out}}$  vs.  $\tau_R$ . Quorum sensing makes  $k_{\text{in}}$  nontrivial, enabling multiple fixed points  $\rho_g$ . For  $\tau_R = 2$ , one has  $k_{\text{out}} \approx 0$ , giving  $\rho_g \approx 0$  (Region I clusters). For  $\tau_R = 128$ , if  $\rho_g \approx \rho_0 = 0.49$  initially, then  $k_{\text{out}} > k_{\text{in}}$ , maintaining  $\rho_g \approx \rho_0$  (Region III, homogeneous). For  $\tau_R = 1024$ , the system flows to a stable fixed point with low  $\rho_g$  (Region II clusters). Fitting parameters  $C = 1.32$  and  $\kappa = 2$  were set by visual comparison of the full phase diagrams.

such effective, initial-condition-dependent phase behavior strongly resembles patterns observed in mussel bed experiments [14, 40].

*Kinetic balance theory*—To properly understand the clustering behavior, we formulate a kinetic theory, following Refs. [30, 46], now for QS interactions. A more detailed derivation is in the SM [41]. The theory calculates the number of particles in each phase in order to derive  $f_c$ . We assume a steady state consisting of a single large cluster at (number) density  $\rho_c$  coexisting with a homogeneous gas of density  $\rho_g$ ; see Fig. 2a. We take the theoretical value  $\rho_c = \frac{2}{\sigma^2\sqrt{3}}$ , corresponding to close packing in a hexagonal arrangement of touching disks [46]. Cluster stability is set by the condition  $k_{\text{out}} = k_{\text{in}}$ , where  $k_{\text{out}}$  and  $k_{\text{in}}$  denote the particle emission and absorption rates per unit length.

To estimate  $k_{\text{in}}$ , we compute the flux of gas particles toward the cluster. Following Ref. [46],  $k_{\text{in}}$  is proportional to the gas density and speed, except that here the self-propulsion speed depends on  $\rho_g$  via QS. This gives [41]

$$k_{\text{in}} = \frac{1}{\pi} \rho_g v(\rho_g^{\text{QS}}), \quad (4)$$

using the local approximation  $v[\tilde{\rho}(\mathbf{r})] \simeq v(\rho)$ . The focal particle perceives a density  $\rho_g^{\text{QS}} = \rho_g - 1/\pi R_{\text{QS}}^2$ , where its own contribution  $1/\pi R_{\text{QS}}^2$  is excluded. Collisions are neglected in the gas, but QS is retained due to its longer interaction range. As a result,  $k_{\text{in}}$  depends



non-monotonically on  $\rho_g$  (Fig. 2b). Such non-monotonic behavior is absent without QS, where  $v = v_0$  [46]. QS thus introduces the following feedback:  $\rho_g$  sets  $v$ , which in turn modifies  $\rho_g$  until a balance is reached. As we will see,  $k_{\text{out}}$  does not depend on  $\rho_g$ . When  $\rho_g > \bar{\rho}$ , gas particles move slower, whereas for  $\rho_g < \bar{\rho}$  they move faster (see Fig. 1b); yet, both cases can yield the same  $k_{\text{in}}$ . This feedback produces up to two stable solutions of  $k_{\text{in}} = k_{\text{out}}$ , corresponding to high- and low-density gases, and hence to two effective equilibrium values of  $f_c$ , obtained below.

To derive an approximation for  $k_{\text{out}}$ , consider a particle at the cluster interface. Once it points outward, the particle starts moving away, but its speed can be very low due to QS. For the particle to escape, we assume it must maintain an outward orientation until it reaches a distance where QS no longer acts. To capture this picture, we take a simple approach. Suppose the particle points at an angle  $\theta$ . If the direction does not change significantly, the particle escapes. The characteristic time for angular reorientation is  $\tau_R$ . Assuming constant  $\theta$ , we define  $T_{\text{QS}}$  as the time required to cross the QS influence zone. The condition for escape is therefore  $T_{\text{QS}} < \tau_R$ .

To estimate  $T_{\text{QS}}$ , we use a simple two-particle scenario, with one particle fixed and the other moving. The speed, denoted  $v_p(r)$ , increases with the interparticle distance  $r$  since the weighted detected density decays with  $r$ . Using the weighting kernel described in the SM [41] and the QS motility  $v(\bar{\rho})$ , we obtain  $v_p(r)$ . In the cluster-particle scenario, only the  $x$ -axis velocity component matters (Fig. 2a), so we take  $v_p(x) \cos \theta$ . We also multiply by a universal fitting constant  $C$  to partially account for our simplified approach. The crossing time is then

$$T_{\text{QS}} = \int_{\sigma}^{R_{\text{QS}}} \frac{dx}{C v_p(x) \cos \theta}. \quad (5)$$

The integral runs from the initial separation,  $x = \sigma$ , up to  $x = R_{\text{QS}}$ , beyond which QS effects vanish.

Below a threshold value of  $\theta$ , escape occurs. At the threshold, one has

$$\tau_R \cos(\pi - \eta) = \int_{\sigma}^{R_{\text{QS}}} \frac{dx}{C v_p(x)}, \quad (6)$$

where  $\eta \in (\frac{\pi}{2}, \pi)$  defines a “escape cone” with half aperture  $\pi - \eta$  (Fig. 2a). We obtain  $\eta$  numerically from Eq. (6).

To proceed with our calculation of  $k_{\text{out}}$ , we follow Ref. [30] by considering the angular probability distribution of particles on the cluster surface and solving a rotational diffusion problem with absorbing boundaries at the edges of the escape cone defined by  $\eta$ . This leads to [41]

$$k_{\text{out}} = \frac{\pi^2 \kappa}{4\sigma \tau_R \eta^2}. \quad (7)$$

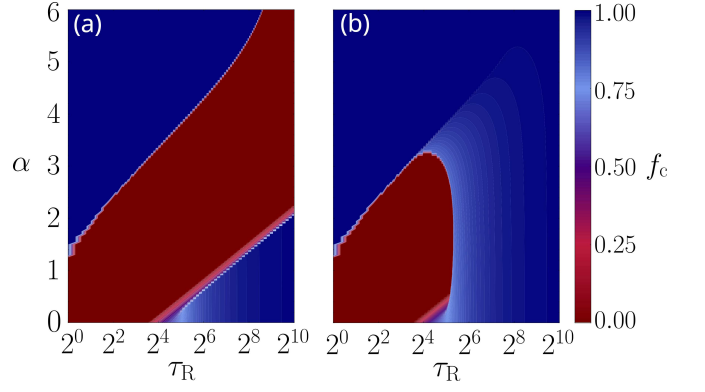


FIG. 3: Effective kinetic balance theory captures key features of the clustering phase diagram. Fraction of particles in clusters  $f_c$  from our theory [Eq. (8)] is shown for (a) homogeneous and (b) clustered initial conditions. The theory reproduces the reentrant clustering and the initial-condition dependence of the diagram, while finer features such as cluster morphology and the pronounced curvature of the transition lines are not resolved.

Here,  $\kappa$  denotes the effective number of particles released per escape event: when one particle escapes, it may trigger an avalanche of further escapes. For simplicity, and following Refs. [30, 46],  $\kappa$  is treated as a universal fitting parameter. We note that, without QS, low  $\tau_R$  leads to high  $k_{\text{out}}$ , whereas with QS, the behavior depends on the functional dependence of  $\eta$  on  $\tau_R$ .

Using  $k_{\text{in}} = k_{\text{out}}$  and conservation of the total number of particles, we can express the clustering order parameter:

$$f_c = \frac{16\phi\eta^2 v(\rho_g^{\text{QS}}) \tau_R - \pi^4 \sigma \kappa}{16\phi\eta^2 v(\rho_g^{\text{QS}}) \tau_R - 2\sqrt{3}\pi^3 \phi \sigma \kappa}. \quad (8)$$

This is the same as the  $f_c$  expression in Ref. [30], except that now  $v(\rho_g^{\text{QS}})$  and  $\eta$  are affected by QS. Figure 3 shows the result. Despite approximations, the theory reproduces both the reentrant and the initial-condition-dependent behaviors. To illustrate how these features arise in the theory, consider  $\alpha = 2$  in Fig. 3a and notice  $k_{\text{in}}(\rho_g)$  in Fig. 2b. For low  $\tau_R$ , particles are too non-persistent and too slow to escape QS, corresponding to a fully closed escape cone ( $\eta = \pi$ ) and  $k_{\text{out}} \approx 0$  (inset of Fig. 2b). This yields  $\rho_g \approx 0$  and  $f_c = 1$ . As  $\tau_R$  crosses a first critical value,  $k_{\text{out}}$  rises sharply (since now  $\pi/2 < \eta < \pi$ ) and the gas will have the global density  $\rho_g \approx \rho_0$ , giving  $f_c \approx 0$ . For sufficient  $\tau_R$ , two solutions emerge. If the system starts near  $\rho_g \approx \rho_0$ , then  $k_{\text{out}} > k_{\text{in}}$  keeps it at the nearby solution,  $\rho_g \approx \rho_0$ : persistence now enables particles to escape QS. If instead the system starts near  $\rho_g \approx 0$ ,  $k_{\text{in}}$  grows with  $\rho_g$  until a low- $\rho_g$  balance is reached, yielding another stable solution. In the simulations, fluctuations not captured by the theory progressively steer regions of the system

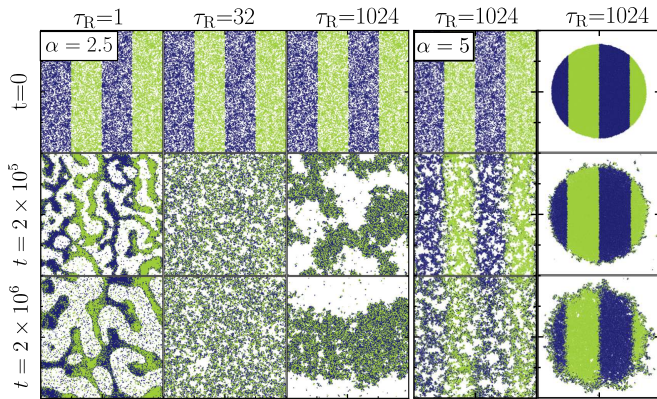


FIG. 4: Quorum-sensing kinetic arrest manifests as suppressed mixing and strong memory of initial conditions. Particles are colored by their initial positions, grouped in vertical stripes with alternating colors. The first, second, and third columns show time evolution for  $\alpha = 2.5$  and  $\tau_R = 1, 32$ , and  $1024$ , respectively. The fourth and fifth columns correspond to  $\alpha = 5$  and  $\tau_R = 1024$ , starting from homogeneous and clustered initial conditions. Preservation of colored stripes over time indicates minimal rearrangement. Mixing slows down with increasing  $\alpha$ , decreasing  $\tau_R$ , or stronger initial clustering.

toward the first solution. Upon further increasing  $\tau_R$  beyond a second critical value, contact-force MIPS lowers  $k_{\text{out}}$  again, restoring  $\rho_g \approx 0$  and  $f_c \approx 1$ , despite the wide open escape cone ( $\eta \approx \pi/2$ ).

*Kinetic arrest*—The physics above stems from the strong motility reduction induced by QS, which produces kinetically arrested configurations. To probe this arrest, we examine the suppression of particle mixing, reflected in a strong memory of initial conditions. Particles are colored by their initial positions in alternating stripes and the system is then evolved (Fig. 4). When QS dominates ( $\alpha = 2.5$ ,  $\tau_R = 1$ ), particles accumulate near their neighbors, forming nearly static microclusters that slowly deform into a gel. The persistence of the initial stripes over long timescales confirms the limited particle motion.

As  $\tau_R$  increases, persistence allows particles to escape QS, causing gels to lose structure. The resulting motility destroys kinetic arrest, as shown by the enhanced mixing for  $\alpha = 2.5$  at  $\tau_R = 32$  and  $1024$  (Fig. 4). By further increasing QS to  $\alpha = 5$  with  $\tau_R = 1024$ , the dynamics exhibit a renewed slowdown. For homogeneous initial states, stripes fade more quickly than for single-cluster initial conditions, where caging delays escape.

*Conclusions*—We have shown how quorum sensing shapes clustering in active matter. The formation of quorum-sensing active gels, which are destroyed when self-propulsion is highly persistent, gives rise to a reentrant clustering phase diagram. Depending on the initial condition, kinetically arrested configurations lead to distinct effective equilibria. A kinetic balance theory

captures both the reentrant behavior and the origin of the two equilibria. Our results highlight parallels between synthetic and biological systems and establish quorum sensing as a key ingredient in active matter self-organization.

Several future directions arise, including the study of non-reciprocal QS interactions [27, 48], the development of a hydrodynamic theory analysis combining QS and steric effects [22], and the exploration of ecological implications of clustering [12, 49]. In addition, models that explicitly include signaling molecules may uncover novel crowding effects. Ultimately, one should compare our results with experiments in bacterial systems [18].

We thank the Brazilian agencies CAPES, CNPq, and FAPESP. L.d.S. was supported by Scholarships No. 140921/2021-4 (CNPq) and No. 88887.911602/2023-00 (CAPES). E.F.T. acknowledges ICTP-SAIFR/IFT-UNESP. P.d.C. was supported by Scholarships No. 2021/10139-2 and No. 2022/13872-5 and ICTP-SAIFR Grant No. 2021/14335-0, all granted by São Paulo Research Foundation (FAPESP), Brazil.

\* [lucas.gabrielsouza@fisica.ufrn.br](mailto:lucas.gabrielsouza@fisica.ufrn.br)

† [teixeiraemanuel9@gmail.com](mailto:teixeiraemanuel9@gmail.com)

‡ [gandhi@fisica.ufrn.br](mailto:gandhi@fisica.ufrn.br)

§ [peter.sollich@uni-goettingen.de](mailto:peter.sollich@uni-goettingen.de)

¶ [pablo.castro@unesp.br](mailto:pablo.castro@unesp.br)

- [1] E. F. Teixeira, H. C. Fernandes, and L. G. Brunnet, *Soft Matter* **17**, 5991 (2021).
- [2] G. Ourique, E. Teixeira, and L. Brunnet, *Physica A: Statistical Mechanics and its Applications* **589**, 126661 (2022).
- [3] W. van Saarloos, V. Vitelli, and Z. Zeravcic, *Soft Matter: Concepts, Phenomena, and Applications* (Princeton University Press, Princeton, NJ, 2024).
- [4] A. Sokolov, I. S. Aranson, J. O. Kessler, and R. E. Goldstein, *Phys. Rev. Lett.* **98**, 158102 (2007).
- [5] E. F. Teixeira, P. de Castro, C. P. Beatrice, H. C. M. Fernandes, and L. G. Brunnet, *arXiv* (2025), 2508.11793 [astro-ph.IM].
- [6] E. F. Teixeira, C. P. Beatrice, H. C. M. Fernandes, and L. G. Brunnet, *Phys. Rev. Lett.* **134**, 138401 (2025).
- [7] M. Ballerini, N. Cabibbo, R. Candelier, A. Cavagna, E. Cisbani, I. Giardina, V. Lecomte, A. Orlandi, G. Parisi, A. Procaccini, M. Viale, and V. Zdravkovic, *Proc. Natl. Acad. Sci. U.S.A.* **105**, 1232 (2008).
- [8] I. Buttinoni, J. Bialké, F. Kümmel, H. Löwen, C. Bechinger, and T. Speck, *Phys. Rev. Lett.* **110**, 238301 (2013).
- [9] S. Henkes, Y. Fily, and M. C. Marchetti, *Phys. Rev. E* **84**, 040301 (2011).
- [10] M. Rojas-Vega, P. de Castro, and R. Soto, *Eur. Phys. J. E* **46**, 1 (2023).
- [11] Y. Fily and M. C. Marchetti, *Phys. Rev. Lett.* **108**, 235702 (2012).
- [12] M. Forget, S. Adiba, L. G. Brunnet, and S. De Monte, *Front. Ecol. Evol.* **10**, 1052309 (2022).

- [13] J. Palacci, S. Sacanna, A. P. Steinberg, D. J. Pine, and P. M. Chaikin, *Science* **339**, 936–940 (2013).
- [14] Q.-X. Liu, A. Doelman, V. Rottschäfer, M. de Jager, P. M. J. Herman, M. Rietkerk, and J. van de Koppel, *Proc. Natl. Acad. Sci. U.S.A.* **110**, 11905 (2013).
- [15] G. Liu, A. Patch, F. Bahar, D. Yllanes, R. D. Welch, M. C. Marchetti, S. Thutupalli, and J. W. Shaevitz, *Phys. Rev. Lett.* **122**, 248102 (2019).
- [16] H. Zhao, A. Košmrlj, and S. S. Datta, *Phys. Rev. Lett.* **131**, 118301 (2023).
- [17] C. Anderson and A. Fernandez-Nieves, *Nat. Commun.* **13**, 1 (2022).
- [18] A. I. Curatolo, N. Zhou, Y. Zhao, C. Liu, A. Daerr, J. Tailleur, and J. Huang, *Nat. Phys.* **16**, 1152 (2020).
- [19] R. Daniels, J. Vanderleyden, and J. Michiels, *FEMS Microbiology Reviews* **28**, 261–289 (2004).
- [20] A. Dal Co, S. van Vliet, D. J. Kiviet, S. Schlegel, and M. Ackermann, *Nat. Ecol. Evol.* **4**, 366 (2020).
- [21] J. van Gestel, T. Bareia, B. Tenenbaum, A. Dal Co, P. Guler, N. Aframian, S. Puyesky, I. Grinberg, G. G. D’Souza, Z. Erez, M. Ackermann, and A. Eldar, *Nat. Commun.* **12**, 1 (2021).
- [22] T. Lefranc, A. Dinelli, C. Fernández-Rico, R. P. A. Dullens, J. Tailleur, and D. Bartolo, *Physical Review X* **15** (2025).
- [23] Q. M. Nguyen, A. Dinelli, G. Spera, and J. Tailleur, arXiv [10.48550/arXiv.2507.08964](https://arxiv.org/abs/10.48550/arXiv.2507.08964) (2025), 2507.08964.
- [24] R. Martínez-García, C. Murgui, E. Hernández-García, and C. López, *PLOS ONE* **10**, e0132261 (2015).
- [25] C. Bechinger, R. Di Leonardo, H. Löwen, C. Reichhardt, G. Volpe, and G. Volpe, *Rev. Mod. Phys.* **88**, 045006 (2016).
- [26] W. J. M. Ridgway, M. P. Dalwadi, P. Pearce, and S. J. Chapman, *Physical Review Letters* **131** (2023).
- [27] A. Dinelli, J. O’Byrne, A. Curatolo, Y. Zhao, P. Sollich, and J. Tailleur, *Nat. Commun.* **14**, 1 (2023).
- [28] J. Tailleur and M. E. Cates, *Phys. Rev. Lett.* **100**, 218103 (2008).
- [29] M. E. Cates and J. Tailleur, *Annu. Rev. Condens. Matter Phys.* , 219 (2015).
- [30] G. S. Redner, A. Baskaran, and M. F. Hagan, *Phys. Rev. E* **88**, 012305 (2013).
- [31] M. Pu, H. Jiang, and Z. Hou, *Soft Matter* **13**, 4112–4121 (2017).
- [32] D. Sarkar, G. Gompper, and J. Elgeti, *Commun. Phys.* **4**, 1 (2021).
- [33] C. M. B. Gutiérrez, C. Vanhille-Campos, F. Alarcón, I. Pagonabarraga, R. Brito, and C. Valeriani, *Soft Matter* **17**, 10479–10491 (2021).
- [34] A. Bhowmick, S. Mitra, and P. K. Mohanty, arXiv (2025), arXiv:2506.05264 [astro-ph.IM].
- [35] T. Bäuerle, A. Fischer, T. Speck, and C. Bechinger, *Nat. Commun.* **9**, 1 (2018).
- [36] A. Fischer, F. Schmid, and T. Speck, *Phys. Rev. E* **101**, 012601 (2020).
- [37] F. Jose, S. K. Anand, and S. P. Singh, *Soft Matter* **17**, 3153 (2021).
- [38] P. N. Segrè, V. Prasad, A. B. Schofield, and D. A. Weitz, *Phys. Rev. Lett.* **86**, 6042 (2001).
- [39] J. Prost, F. Jülicher, and J.-F. Joanny, *Nature Physics* **11**, 111–117 (2015).
- [40] J. van de Koppel, J. C. Gascoigne, G. Theraulaz, M. Rietkerk, W. M. Mooij, and P. M. J. Herman, *Science* **322**, 739 (2008).
- [41] SM, See Supplemental Material at [URL] for details of the simulations, derivations and additional figures.
- [42] H. Tong and H. Tanaka, *Nat. Commun.* **10**, 1 (2019).
- [43] Y. Duan, J. Agudo-Canalejo, R. Golestanian, and B. Mahault, *Phys. Rev. Lett.* **131**, 148301 (2023).
- [44] A. Villa-Torrealba, C. Chávez-Raby, P. de Castro, and R. Soto, *Physical Review E* **101**, 062607 (2020).
- [45] C. Merrigan, K. Ramola, R. Chatterjee, N. Segall, Y. Shokef, and B. Chakraborty, *Phys. Rev. Res.* **2**, 013260 (2020).
- [46] G. S. Redner, M. F. Hagan, and A. Baskaran, *Phys. Rev. Lett.* **110**, 055701 (2013).
- [47] A. K. Omar, K. Klymko, T. GrandPre, and P. L. Geissler, *Phys. Rev. Lett.* **126**, 188002 (2021).
- [48] J. Agudo-Canalejo and R. Golestanian, *Phys. Rev. Lett.* **123**, 018101 (2019).
- [49] D. R. Zusman, A. E. Scott, Z. Yang, and J. R. Kirby, *Nature Reviews Microbiology* **5**, 862 (2007).

# Supplemental Material for “How Quorum Sensing Shapes Clustering in Active Matter”

L. de Souza,<sup>1,2,\*</sup> E. F. Teixeira,<sup>3,†</sup> G. M. Viswanathan,<sup>1,4,‡</sup> P. Sollich,<sup>2,5,§</sup> and P. de Castro<sup>6,¶</sup>

<sup>1</sup>*Departamento de Física Teórica e Experimental,  
Universidade Federal do Rio Grande do Norte. Natal 59078-970, Brazil*

<sup>2</sup>*Institut für Theoretische Physik, University of Göttingen,  
Friedrich-Hund-Platz 1, 37077 Göttingen, Germany*

<sup>3</sup>*Instituto de Física, Universidade Federal do Rio Grande do Sul. Porto Alegre 91501-970, Brazil*

<sup>4</sup>*National Institute of Science and Technology of Complex Systems,  
Federal University of Rio Grande do Norte. Natal 59078-900, Brazil*

<sup>5</sup>*Department of Mathematics, King's College London. London WC2R 2LS, UK*

<sup>6</sup>*ICTP South American Institute for Fundamental Research,  
Instituto de Física Teórica, Universidade Estadual Paulista– UNESP, São Paulo, Brazil*

(Dated: December 3, 2025)

This Supplementary Material contains details on the simulations performed, the kinetic theory derivation, and the description of the supplementary movies. We also compare simulations starting with different initial conditions to show that they converge to the same final state only on very long timescales. Moreover, we present results for extremely high QS strength.

## I. SIMULATION DETAILS

Throughout the simulations, we set  $v_1 = 10^{-4}v_0$ , where  $v_0 = 1$ , and the translational diffusion constant is fixed at  $D_T = 5 \times 10^{-6}$ . In this regime, kinetic arrest effects are present, but thermal fluctuations become relevant once we get to very long timescales. The repulsion elastic constant  $k$  is chosen such that particles overlap at most 3% of  $\sigma$  under the action of the self-propulsion forces. Explicitly, we set  $\mu k \times (0.03\sigma) = v_0$ , corresponding to  $\mu k \approx 30v_0/\sigma$  [1]. The QS parameters are  $R_{QS} = 1.5\sigma$ ,  $\bar{\rho} = 0.1$ , and  $\delta\rho = 0.05$ . We set  $\bar{\rho}$  so that a single particle within the QS range is sufficient to activate motility reduction. Notice that our value of  $R_{QS} = 1.5\sigma$  is not so large. This agrees with experiments showing that, at moderate densities, the QS range is reduced due to absorption of signaling molecules. [2, 3].

We employ the Euler-Maruyama method with a time step calculated by considering an extreme interaction case. In the absence of quorum sensing, we require that a particle will move by at most  $0.1\sigma$  when interacting with two particles overlapping with it by the same length. This results in the minimum time step  $\Delta t_{\min} = \frac{0.1\sigma}{v_0 + 2\mu k \times (0.1\sigma)}$ . Rounding up  $\Delta t_{\min}$  for our parameters, we obtain  $\Delta t = 0.01$ .

The distance-weighted density detected by each particle is defined as  $\tilde{\rho}(\mathbf{r}) = \int K(\mathbf{r} - \mathbf{r}')\rho(\mathbf{r}')d^2\mathbf{r}'$ , where we assume each particle is a point source,  $\rho(\mathbf{r}) = \sum_{i=1}^N \delta(\mathbf{r} - \mathbf{r}_i)$ . Within the interaction range  $R_{QS}$ , each particle is weighted by the interparticle distance using the kernel [4]

$$K(\mathbf{r}) = Z^{-1} \exp\left(-\frac{1}{1 - (r/R_{QS})^2}\right) \Theta(1 - r/R_{QS}), \quad (1)$$

where  $Z = 0.1485\pi R_{QS}^2$ . Hence, for the  $i$ th particle, the detected density is

$$\tilde{\rho}(\mathbf{r}_i) = \sum_{j \neq i} K(\mathbf{r}_i - \mathbf{r}_j). \quad (2)$$

Finally, the mean value of  $f_c$  was computed from the final 30% of the time series.

## II. EXTREMELY LONG TIMESCALES

Fig. S1 shows the system evolution over long relaxation timescales for the homogeneous and clustered initial conditions. Starting from a homogeneous configuration in parameter Region III, particles end up colliding with each

---

\* [lucas.gabrielsouza@fisica.ufrn.br](mailto:lucas.gabrielsouza@fisica.ufrn.br)

† [teixeiraemanuel9@gmail.com](mailto:teixeiraemanuel9@gmail.com)

‡ [gandhi@fisica.ufrn.br](mailto:gandhi@fisica.ufrn.br)

§ [peter.sollich@uni-goettingen.de](mailto:peter.sollich@uni-goettingen.de)

¶ [pablo.castro@unesp.br](mailto:pablo.castro@unesp.br)



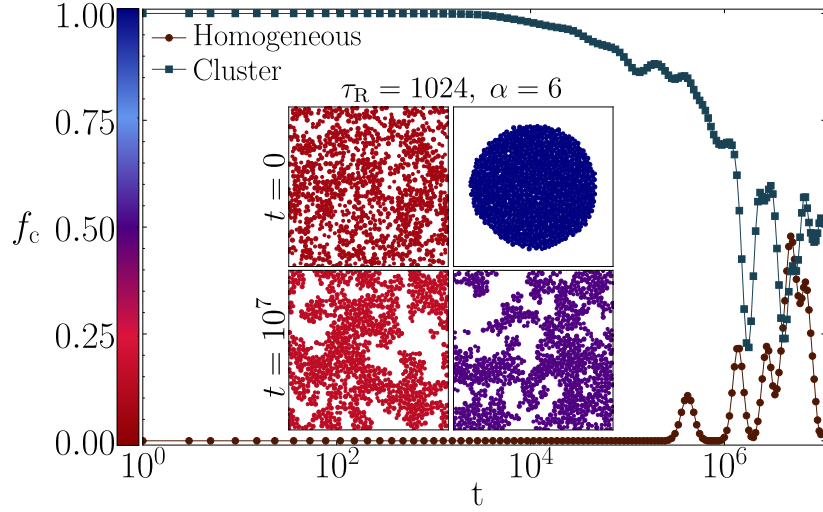


FIG. S1: Different initial conditions converge to similar final states over long relaxation timescales. Evolution of the system with  $N = 10^3$ , for homogeneous and single-cluster initial conditions. Here,  $\tau_R = 1024$  and  $\alpha = 6$  (Region III in Fig. 1d). In the main plot, we show the time series of  $f_c$ , smoothed using a Gaussian filter with standard deviation equal to the time separation between two sequential data points. The color bar denotes the  $f_c$  mean value. Inset shows snapshots. We note that  $f_c$  for both initial conditions converges to similar values, considering fluctuations. The final states are nearly homogeneous phases, with some degree of clustering. The minimum speed  $v_1$  and the thermal diffusion help particles to escape from the cluster interface, eventually leading to the evaporation of the single-cluster into an amorphous clustering state. For  $t \approx 10^7$ , the system loses memory of the initial condition.

other very soon and forming small stable clusters, which persist for long timescales due to high persistence time and QS motility reduction. This results in a nearly homogeneous phase, with a small degree of clustering. If the system starts from a single-cluster initial condition, the same proceeds, albeit over much longer timescales. As particles eventually escape from the cluster interface, they interact in the gas, forming again small, long-lived clusters. Progressively, more particles escape, ultimately leading to the complete evaporation of the initial cluster. These relaxation timescales grow with the number of particles.

### III. DETAILS OF THE KINETIC BALANCE THEORY

Here, we give details of the derivation of our kinetic theory for QS particles, which is based on Ref. [5]. For completeness, we provide even those details that do not change due to QS.

We assume a large single closed-packed cluster. First, we calculate the rate of particle absorption per length of the interface,  $k_{\text{in}}$ . For particles moving in the gas phase with orientation  $\theta$ ,  $k_{\text{in}}(\theta)$  should be proportional to the gas density  $\rho_g$  and the particle speed component in the  $x$ -axis. Differently from Ref. [5], our particle speed depends on the density detected via QS,  $\rho_g^{\text{QS}}$ , where  $\rho_g^{\text{QS}} = \rho_g - 1/\pi R_{\text{QS}}^2$ , as discussed in the main text. Hence,  $k_{\text{in}}(\theta) = \rho_g v(\rho_g^{\text{QS}}) \cos \theta$ . To calculate the angular average of  $k_{\text{in}}(\theta)$  that gives the total cluster influx per unit length, we first divide by  $2\pi$  to normalize and then integrate from  $-\pi/2$  to  $\pi/2$ . This leads to

$$k_{\text{in}} = \frac{1}{\pi} \rho_g v(\rho_g^{\text{QS}}). \quad (3)$$

The total particle escape rate per unit length,  $k_{\text{out}}$ , can be written as

$$k_{\text{out}} = -\frac{1}{\sigma} \partial_t \int_{-\eta}^{\eta} P(\theta, t) d\theta \Big|_{t=0}, \quad (4)$$

where  $P(\theta, t)$  is the particle orientation distribution on the cluster interface, which evolves according to the rotational diffusion equation

$$\partial_t P(\theta, t) = \tau_R^{-1} \partial_\theta^2 P(\theta, t). \quad (5)$$



We have absorbing boundary conditions  $P(\pm\eta, t) = 0$ , where  $\eta$  is the complementary angle of the kinetic escape cone discussed in the main text. Its general solution is given by  $P(\theta, t) = \sum_{n=1}^{\infty} A_n \cos\left(\frac{\pi n \theta}{2\eta}\right) e^{-\frac{n^2 \pi^2}{4\eta^2} \frac{t}{\tau_R}}$ . We observe that the time decay is dominated by the first term when the system is in a steady state. Normalizing the solution, we find

$$P(\theta, t) \approx \frac{\pi}{4\eta} \cos\left(\frac{\pi}{2\eta}\theta\right) \exp\left(-\frac{\pi^2}{4\eta^2} \frac{t}{\tau_R}\right). \quad (6)$$

Additionally, we need to account for the particle escape avalanches, controlled by the fitting parameter  $\kappa$ . Thus, inserting Eq. (6) into Eq. (4) and multiplying by  $\kappa$ , we find

$$k_{\text{out}} = \frac{\pi^2 \kappa}{4\sigma\eta^2 \tau_R}. \quad (7)$$

#### IV. SUPPLEMENTARY MOVIES

Below, we describe the supplementary movies. With the exception of  $\delta\rho = 0.05$ ,  $v_1 = 10^{-4}v_0$  and  $D_T = 5 \times 10^{-6}$ , the parameters used are indicated. The movies can be found [here](#).

**Movie S1:** Simulation showing the competition between quorum-sensing motility reduction and persistent motion. Red arrows denote the particles' polarities. Particles are colored by their quorum-sensing speed; see colorbar. The orange circles show the quorum-sensing interaction region, with radius  $R_{\text{QS}}$ . Parameters:  $\phi = 0.1$ ,  $N = 50$ ,  $\bar{\rho} = 0.1$ ,  $\tau_R = 16$ , and  $\alpha = 3$ .

**Movie S2:** Simulations showing evolution and steady state for the different regions of the phase diagram with homogeneous initial conditions. The panels correspond (from left to right) to  $\tau_R = 1, \alpha = 5$  (Region I),  $\tau_R = 32, \alpha = 2.5$  (Region III),  $\tau_R = 1024, \alpha = 1$  (Region II). Particles are colored by their quorum-sensing speed; see colorbar. Parameters:  $\phi = 0.4$ ,  $N = 2 \times 10^4$ ,  $\bar{\rho} = 0.1$ .

**Movie S3:** Simulations showing evolution for different initial conditions. Despite long-lived transient states, both cases eventually converge to the same state for long enough relaxation timescales. Here, we use only  $N = 10^3$  be able to access such timescales. For  $t = 10^7$ , the system loses memory of its initial condition as kinetic arrest fades away. Particles are colored by their quorum-sensing speed; see colorbar. The orange circles show the quorum-sensing interaction region, with radius  $R_{\text{QS}}$ . Parameters:  $\phi = 0.4$ ,  $N = 10^3$ ,  $\bar{\rho} = 0.1$ ,  $\tau_R = 1024$ ,  $\alpha = 6$ .

- 
- [1] Y. Fily and M. C. Marchetti, Athermal Phase Separation of Self-Propelled Particles with No Alignment, [Phys. Rev. Lett.](#) **108**, 235702 (2012).
  - [2] A. Dal Co, S. van Vliet, D. J. Kiviet, S. Schlegel, and M. Ackermann, Short-range interactions govern the dynamics and functions of microbial communities, [Nat. Ecol. Evol.](#) **4**, 366 (2020).
  - [3] D. M. Gordon, R. E. Paul, and K. Thorpe, What is the function of encounter patterns in ant colonies?, [Anim. Behav.](#) **45**, 1083 (1993).
  - [4] J. O'Byrne, A. Solon, J. Tailleur, and Y. Zhao, An Introduction to Motility-Induced Phase Separation, [arXiv 10.1039/9781839169465](#) (2021), 2112.03979.
  - [5] G. S. Redner, M. F. Hagan, and A. Baskaran, Structure and Dynamics of a Phase-Separating Active Colloidal Fluid, [Phys. Rev. Lett.](#) **110**, 055701 (2013).